Monthly Notices
of the
ROYAL ASTRONOMICAL SOCIETY

Mon. Not. R. Astron. Soc. **404,** 1121–1128 (2010) doi:10.1111/j.1365-2966.2010.16357.x

Evolution of the spectrum and VLBI structure of W75N during the huge OH maser flare in 2003–2007

V. I. Slysh,[1⋆]† A. V. Alakoz[1⋆] and V. Migenes[2,3⋆]

[1]*Astro Space Centre, Lebedev Physical Institute, Profsoyuznaya str. 84/32, Moscow 117997, Russia*
[2]*Departamento de Astronomia, Universidad de Guanajuato, Apdo. Postal 144, Guanajuato, CP 36000, GTO Mexico*
[3]*Department of Physics and Astronomy, Brigham Young University, ESC-N145, Provo, Utah 84602*

Accepted 2010 January 13. Received 2010 January 13; in original form 2009 June 1

ABSTRACT

We present results of single-dish and very long baseline interferometry (VLBI) observations of a strong 1000-Jy OH maser flare in the star-forming region W75N. The flare was first seen in 2003, and persisted for at least four years. Three major spectral features were present during the whole period of observations, with N_1 being the strongest initially and N_2 becoming stronger later. The large velocity range of 43 km s^{-1} observed during the flare is not kinematic in origin, but is caused by the Zeeman splitting in the strong magnetic field generated by the central star. The maps and proper motion of the maser spots were monitored over eight epochs, between 1998 and 2006, using the European VLBI Network (EVN) supplemented by published Very Large Baseline Array (VLBA) data. Mapping of the maser spots has shown that all the new spectral features of the flare were located close to the ultracompact H II region VLA2, while the quiescent maser features were found near VLA1. We suggest that the flare was initiated by a disturbance, probably an magnetohydrodynamic (MHD) shock launched from the massive young star, also responsible for the excitation of the ultracompact H II region. The proper motion of the majority of the maser spots was not detected at 1665 and 1667 MHz with the upper limit of several km s^{-1}. The only positive detection of the proper motion was made for the two brightest flare features N_1 and N_2. The spot N_2 is moving along the filamentary spot N_3, with a tangential velocity of 14 km s^{-1}. This motion is caused by the MHD shock propagating along the filament. The measured low upper limit for the velocity of OH maser spots is consistent with models of a slowly rotating Keplerian disc rather than with outflows, jets or expanding shells.

Key words: magnetic fields – masers – stars: formation – ISM: individual: W75N – ISM: kinematics and dynamics.

1 INTRODUCTION

W75N is a star-forming region in which formation of at least three massive stars is spotted through continuum emission from ultracompact H II regions VLA1–3 detected with the Very Large Array (VLA) by Torrelles et al. (1997). The star formation process is accompanied by the maser emission in OH, H_2O and CH_3OH lines. The OH maser emission in W75N has several distinct features not found in the majority of other OH maser sources. It underwent a unique huge flare of emission at 1665 MHz in 2003 that made it for a time the brightest OH maser in the sky ever observed (Alakoz et al. 2005). The emission of many spectral features has a high degree of linear polarization, with no visible Zeeman splitting pattern, also there are several circularly polarized Zeeman pairs of σ components (Slysh et al. 2002; Fish et al. 2005; Slysh & Migenes 2006; Fish & Reid 2007). During the precursor flare in 2000 a strong magnetic field was measured (Slysh & Migenes 2006; Fish & Reid 2007), an order of magnitude higher than typical magnetic field strength in OH masers. Maser spots of both emission flare and those with enhanced magnetic field were found close to the ultracompact H II region VLA2. The rest of the maser spots are related to VLA1; they are less variable and show normal magnetic field strength. H_2O masers are present near both VLA1 and VLA2 and experience strong flux variations (Lekht, Slysh & Krasnov 2007). Methanol masers were found only near VLA1, and show low variability (Minier, Booth & Conway 2000; Goedhart, Gaylard & van der Walt 2004).

The origin of occasional maser emission flares is not well understood (Goddi et al. 2006). The location of flaring maser spots close to the ultracompact H II region may be an indication of the central

⋆E-mail: vslysh@asc.rssi.ru (VIS); rett@asc.rssi.ru (AVA); vmigenes@byu.edu (VM)

†Dr. Slysh passed away just before submitting this manuscript. His accomplishments in the fields of radio astronomy. star formation and maser physics, among others, were many and significant. Slava will be missed.

young massive star, hidden inside the ultracompact H II region, as a driver of disturbances travelling to nearby pre-existing gas clumps. The passage of a disturbance, that can be a magnetohydrodynamic (MHD) shock, causes an increase of the maser emission. In another model, it is assumed that the maser spots are located in expanding shells or ionization fronts and move with them. The sudden flashes of the maser emission are not expected in this model. A different model of maser emission flares assumes a chance alignment in the direction of the line of sight of two moving clumps, with moderate maser gain. In the non-linear unsaturated regime, this can produce an increase in the maser gain which can be much larger than a factor of 2. The turbulent maser models do not need discrete gas clumps. The maser emission is formed in the turbulent medium of molecular clouds along lines of sight which provide a chance coherence for radial velocities, required for the maser amplification.

In order to get insight into the nature of maser emission sources, we exploited the opportunity of occurrence of two strong OH maser emission flares in W75N. We have used different telescopes and arrays for monitoring the spectrum, polarization and position of the maser spots during the evolution of the flares. A similar study of W75N OH maser during this flare was made by Fish & Reid (2007), with a lower time sampling.

2 OBSERVATIONS AND DATA REDUCTION

The first single-dish observations of the OH maser flare were carried out with the Nancay radio telescope in 2003 October, and subsequently with the 64-m telescope in Kalyazin. Details of the initial spectral monitoring with the Kalyazin telescope were given in Alakoz et al. (2005). The Kalyazin observations were conducted in the dual-circular polarization mode. Here, we report results of extensive monitoring for the period from 2004 July to 2007 July, taken at nine epochs, with the same correlator setup.[1] very long baseline interferometry (VLBI) observations were carried out with the European VLBI Network (EVN) on three epochs, in 2005 November, and in 2006 March and June. The synthesized beam size was approximately $10 \times 6\,\mathrm{mas}^2$. Additionally, published results from VLBA observations in 1998 July (Slysh et al. 2002), 2001 January (Slysh & Migenes 2006; Fish et al. 2005) and 2004 September (Fish & Reid 2007) were used for the proper motion measurements for a total of six epochs distributed over an 8-yr period. The spectral resolution of the VLBI observations was $0.176\,\mathrm{km\,s^{-1}}$, and the observations were conducted in the full polarization mode, except VLBA observations in 2004 which were taken in dual-circular polarization mode. The maser maps were made using standard task IMAGR of the National Radio Astronomy Observatory (NRAO)[2] AIPS package, and individual maser spots were searched for on VLBI maps, fitted with two-dimensional Gaussians, and deconvolved for the synthesized beam smearing with the task SAD of AIPS. The full list of spots detected in at least two epochs is given in Table 1 for the 1665 MHz transition and Table 2 for the 1667 MHz transition (polarization data have been omitted and reserved for a further publication).

[1] There is a published spectrum of 1665 MHz OH line taken with Urumqui radio telescope on 2004 May 7 during the test of receiver, two months before the first Kalyazin observation (Zhang et al. 2005). After correction for a radial velocity shift of $-3\,\mathrm{km\,s^{-1}}$ and an amplitude calibration by a factor of 2, the Urumqui spectrum is similar to the first 1665 MHz Kalyazin spectrum.

[2] NRAO is a facility of the National Science Foundation operated under cooperative agreement by Associated Universities, INC.

3 RESULTS

3.1 Spectral variations

Overlaid 11-epoch colour-coded single-dish Kalyazin right-hand circular (RHC) 1665 MHz spectra of W75N and three-epoch 1667 MHz spectra, obtained after the onset of the huge flare are shown in Figs 1 and 2.

All spectra were normalized to the radial velocity and amplitude of the feature *A*.[3] The flux of feature *A* remained unchanged within about 5 per cent through this period from its 1998 strength. The normalization corrections ranged on average from 10 to 50 per cent, except for flaring features. In addition to the spectral features that were present in the earlier quiescent state in 1998 (Slysh, Val'tts & Migenes 2001; Slysh et al. 2002), the flare spectra show new strong features, as well as many weaker ones. Some of them are similar to the so-called 'Elder transient' features, or high velocity (HV) features (Yngvesson et al. 1975), located outside the standard spectrum, at high positive velocities and RHC polarized (Fig. 3).

There is also one feature at the high negative velocity $-12.48\,\mathrm{km\,s^{-1}}$, which is left-hand circular (LHC) polarized. In the first spectrum, a feature named N_1 is the strongest reaching about 1000 Jy. The features N_2 and N_3 are much weaker. Gradually N_1 has weakened, and N_2 became the strongest, with the flux exceeding 1000 Jy. At later epochs additional features N_4 and N_5 emerged near *A* and N_1, respectively. Over the whole period only the amplitude and polarization of features varied significantly, the radial velocity remaining constant. The radial velocity of weak HV features also did not change, while the amplitude varied over a large range. The polarization status of the HV features always remained unchanged. Standard features $A - H$ of the quiescent state did not change much. The 1667-MHz spectrum shows many new features which were not present before the flare. Some of the old 1667-MHz strong features have disappeared or became very weak after the flare. HV features are present at the positive velocity side of the spectrum, at about the same velocities as 1665-MHz HV features. They are also RHC polarized. However, the intensity of 1667-MHz features is in general lower than the 1665-MHz features. No single big feature, with the flux above 5 Jy is present in 1667-MHz spectrum. The strongest, elliptically polarized feature *L* (Slysh et al. 2002) which was about 50-Jy strong in 1998 and 2001, has faded to 1 Jy in 2003 October. The three other 1667 MHz features in 1998 spectrum *M*, *N* and *O* also weakened substantially. Similarly, the two strong extended features *J* and *K* in 1665-MHz spectrum of 1998, with the flux density 20–30 Jy later became an order of magnitude weaker.

3.2 Proper motion of the maser spots

3.2.1 Absolute position

In the first EVN run, 2005 September, we used phase-referencing in order to determine absolute position of the OH maser W75N. We choose feature *A* as a reference for the rest of the maser spots, so the absolute position of *A* has been measured. The reference source was the VLBA calibrator J2052+3635, a double source with component separation about 50 mas, with a position known to within 0.56 mas. For the position measurement, we have mapped the calibrator in one channel of the *line* file, using self-calibration on one of the

[3] Notation of the maser features is from Slysh et al. (2002).

Table 1. 1665 MHz maser spots detected in at least two epochs. Coordinates are in milliarcseconds relative to the reference spot *A* at 12.45 km s^{-1}.

	July	1998	January	2001	September	2004	November	2005	March	2006	June	2006
V, km s^{-1}	α	δ	α	δ	α	δ	α	δ	α	δ	α	δ
30.32	–	–	–	–	–	–	778.86	–96.15	778.13	–95.08	–	–
26.81	–	–	–	–	–	–	736.90	−129.63	736.63	−131.45	735.26	−131.54
26.41	–	–	–	–	–	–	752.81	−88.31	752.16	−88.08	752.66	−87.26
25.87	–	–	–	–	–	–	737.94	−139.49	737.98	−140.15	–	-
24.30	–	–	–	–	–	–	727.72	−144.11	725.66	−143.19	–	-
17.35	–	–	–	–	–	–	734.70	−173.87	729.28	−173.02	727.45	−173.31
16.35	–	–	–	–	1784.05	−587.70	1783.44	−587.06	1781.38	−591.67	1781.24	−587.91
14.60	–	–	–	–	326.40	130.44	325.96	132.88	325.84	131.81	324.01	132.09
13.90	–	–	91.71	−72.40	91.59	−70.41	91.83	−70.64	91.03	−70.56	89.66	−70.16
12.98	–	–	139.83	−15.41	139.41	−14.31	139.19	−13.22	138.97	−13.90	137.38	−14.00
12.87	–	–	–	–	–	–	−261.29	−313.24	−261.40	−313.45	−260.93	−315.15
12.84	–	–	128.96	−54.63	128.99	−58.49	–	–	–	–	127.79	−65.03
12.45	0.00	0.00	0.00	0.00	0.00	0.00	0.00	0.00	0.00	0.00	0.00	0.00
12.25	–	–	–	–	–	–	1785.00	−594.00	1789.20	−594.48	1786.24	−592.94
11.52	–	–	–	–	–	–	730.15	−193.27	730.17	−194.35	728.29	−194.49
10.97	–	–	200.07	705.97	200.83	707.17	200.07	708.11	200.20	707.84	198.57	709.59
10.16	–	–	–	–	231.73	549.57	232.01	553.91	232.20	553.20	230.26	553.39
9.89	–	–	–	–	233.17	559.34	232.52	561.74	232.23	560.67	230.70	560.81
9.84	–	–	−247.10	−1143.14	−248.03	−1145.15	−249.06	−1147.15	−247.79	−1142.89	–	-
9.57	–	–	118.89	−71.52	115.68	−71.19	115.66	−70.80	116.20	−71.44	116.60	−70.91
9.36	203.20	603.50	204.48	603.59	205.45	605.48	204.90	606.71	204.84	605.86	203.36	606.65
8.23	–	–	–	–	−109.23	710.49	−110.75	710.20	−108.52	709.80	–	-
7.35	300.40	1144.30	300.58	1145.27	300.93	1147.44	–	–	–	–	–	-
7.35	–	–	−490.03	−442.59	−492.90	−443.27	−490.74	−448.53	−493.62	−443.01	–	-
7.29	488.30	1344.10	488.75	1345.88	489.70	1348.06	487.76	1353.39	488.09	1349.60	485.87	1350.37
6.90	–	–	296.99	1109.57	297.00	1110.60	295.82	1112.39	295.60	1111.33	295.94	1111.27
6.74	–	–	–	–	767.67	−89.94	755.49	−88.06	755.56	−86.77	753.90	−83.13
6.58	–	–	342.32	1131.16	342.95	1133.38	342.38	1135.02	342.14	1133.94	342.85	1133.98
6.20	–	–	278.59	1094.35	279.16	1097.03	278.90	1096.80	–	–	–	-
6.00	–	–	−295.89	254.63	−298.30	256.03	−299.98	256.45	−299.78	255.98	−303.58	256.97
5.95	–	–	–	–	791.86	−240.99	792.53	−238.68	791.90	−239.55	790.95	−239.99
5.88	178.70	513.40	178.03	512.65	–	–	–	–	–	–	–	-
5.84	–	–	278.59	1094.45	277.31	1093.80	274.61	1094.24	276.81	1094.67	273.02	1093.70
5.80	301.40	1177.00	301.67	1177.13	301.63	1178.02	300.23	1180.85	300.06	1178.84	298.13	1178.83
5.57	–	–	343.06	1175.81	344.99	1178.37	341.18	1179.41	341.48	1178.90	340.05	1178.55
5.56	–	–	206.58	1100.24	206.32	1102.04	204.86	1103.65	204.83	1102.44	203.15	1102.61
5.52	–	–	230.37	580.81	230.70	581.16	229.76	581.85	230.15	582.08	227.45	581.14
5.31	456.90	1291.20	457.55	1292.30	457.51	1293.18	456.26	1295.18	456.20	1294.29	453.66	1293.83
5.25	488.30	1344.10	488.75	1345.88	489.66	1348.14	488.21	1350.37	487.35	1348.60	485.33	1349.87
4.19	–	–	282.57	1112.98	282.86	1110.75	281.55	1115.52	281.01	1114.50	279.90	1117.89
3.82	550.40	1494.90	550.65	1494.67	550.46	1496.68	–	–	548.95	1498.40	547.63	1499.03
2.73	–	–	–	–	–	–	747.64	−139.38	745.65	−140.11	744.78	−140.03
2.11	–	–	–	–	739.49	−145.81	740.46	−145.12	740.20	−146.50	739.00	−146.33
1.12	–	–	–	–	–	–	814.21	−113.71	812.27	−114.98	–	-
0.32	–	–	–	–	744.33	−133.87	744.18	−132.27	743.98	−132.66	742.08	−131.75
−0.64	–	–	–	–	743.11	−130.81	743.35	−129.37	743.08	−127.38	742.91	−121.89
−3.72	–	–	–	–	–	–	–	–	754.05	−125.73	752.48	−124.68
−12.48	–	–	–	–	–	–	907.09	−59.55	906.65	−61.20	–	–

bright maser spots. The position of the two calibrator components was determined from Gaussian fits with AIPS task SAD. The western component is the position calibrator, and we have measured the offset of the maser spot *A* from this component. Applying the offset to the assumed position of the maser, we obtained the absolute position of feature *A*: RA = $20^{\rm h}38^{\rm m}36\overset{\rm s}{.}4082$, Dec. = $42^\circ37'34\overset{''}{.}238$ (±2 mas) (J2000). This position is consistent with the position determined with the AIPS fringe-rate method task FRMAP earlier (Slysh & Migenes 2006) and is more accurate, by at least an order of magnitude.

3.2.2 *Proper motion*

The VLBI map of 1665- and 1667-MHz maser spots of W75N, based on Tables 1 and 2 data is presented in Fig. 4, where position of ultracompact H II regions VLA1 and VLA2 (Shepherd, Kurtz & Testi 2004) is also shown.

All maser spots near VLA2 are new, see Fig. 5, and were not present before the onset of the huge flare, even during the precursor flare of 2000, while those near VLA1 were present almost at all epochs. It is evident from this map and similar maps from other

Table 2. 1667 MHz maser spots detected in at least two epochs. Coordinates are in milliarcseconds relative to 1665 MHz spot *A* at 12.45 km s^{-1}.

V, km s^{-1}	α	δ	α	δ	α	δ	α	δ	α	δ	α	δ
21.55	–	–	–	–	–	–	757.15	−91.77	756.9	−90.18	757.35	−90.63
14.97	–	–	–	–	–	–	762.11	−80.39	762.7	−79.45	763	−79.08
14.4	–	–	1784.19	−583.45	1784.15	−582.29	1785.78	−582.44	1786.39	−581.02	1784.49	−581.58
13.74	–	–	1830.9	−562.83	1833.64	−559.6	1834.69	−558.86	1836.58	−557.91	1835.8	−557.27
12.65	–	–	130.02	−54.01	129.7	−54.8	128.39	−54.8	130.36	−54.45	130.41	−54.45
10.6	–	–	–	–	758.52	−90.35	755.88	−88.8	758.29	−85.9	–	–
10.19	–	–	106.49	211.58	105.78	211.8	105.78	211.8	105.78	211.8	105.78	211.8
10.00	–	–	201.13	707.02	202.42	708.63	202.38	708.06	202.6	710.31	202.99	709.95
8.08	–	–	196.45	593.57	197.78	595.08	196.64	595.11	–	–	198.35	596.43
8.07	207.5	673.78	207.63	672.66	207.81	673.79	207.81	672.53	207.8	675.42	207.84	675.36
6.5	–	–	–	–	233.66	550.95	234.41	553.12	234.53	552.58	234.37	552.33
6.02	221.2	653.08	221.98	652.34	222.44	655.77	221.6	657.25	222.62	657.26	222.94	657.36
6.01	–	–	–	–	–	–	752.37	−159.69	752.67	−159.16	752.8	−158.1
5.63	–	–	490.9	1348.48	491.93	1351.43	490.88	1352.26	490.59	1352.4	491.72	1353.1
5.44	207.4	674.88	207.38	673.45	207.18	674.5	207.08	674.72	207.75	675.62	208.54	675.76
5.30	–	–	–	–	–	–	745.52	−133.97	746.48	−131.98	746.92	−131.11
5.25	–	–	–	–	219.18	618.12	220.29	617.47	–	–	220.84	618.4

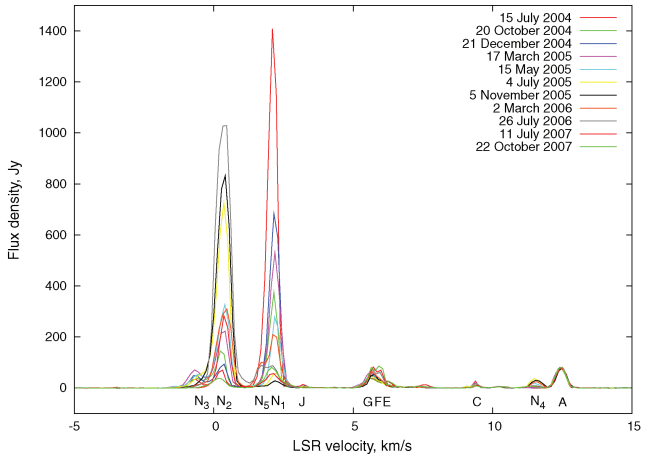

Figure 1. Overlaid colour-coded spectra of W75N in RHC 1665 MHz OH line between 2005 and 2007.

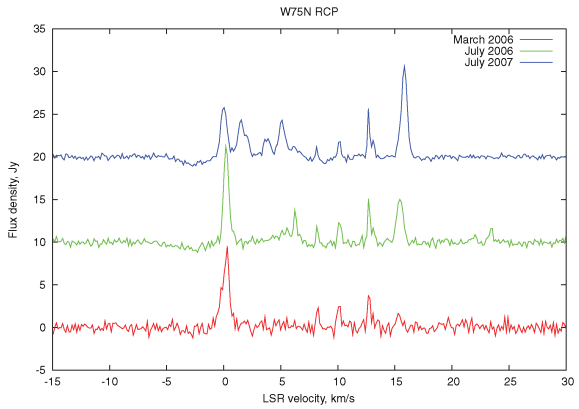

Figure 2. Three spectra of W75N in 1667 MHz RHC OH line between 2005 and 2007.

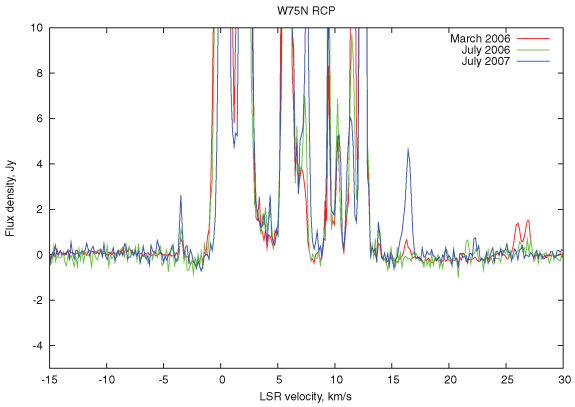

Figure 3. HV features in 1665 MHz RHC.

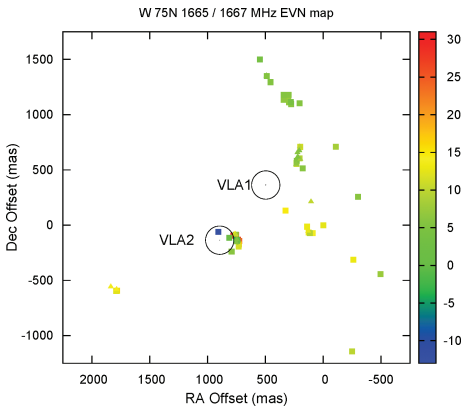

Figure 4. Map of W75N 1665 MHz maser spots. Mainly from 2006 March but in addition some spots only detected in November 2005 and July 2006, were included.

epochs that all strongly variable features including the strongest N_1 and N_2 and HV features are found near VLA2.

The proper motion of the maser spots has been measured relative to the reference maser feature *A* at 12.45 km s^{-1}. The largest time-span between measured epochs was 93 months, or 8 yr, from 1998 July to 2006 June, and consisted of six epochs. 48 maser spots at 1665 MHz and 17 spots at 1667 MHz were observed at least on two epochs (the full list of multi-epoch maser spots is given in Table 1). The precision of the transverse velocity measurements of the individual maser spots varied from about 10 μas per month

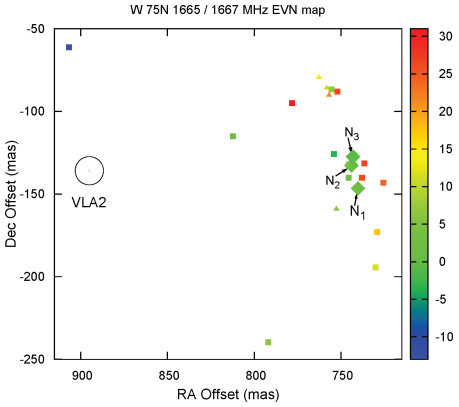

Figure 5. Map of W75N maser spots near VLA2. Mainly from March 2006 but in addition some spots only detected in 2005 November and 2006 July were included.

(1.15 km s^{-1} at the assumed distance 2 kpc) to 200 μas per month (23 km s^{-1}), depending on the time-span between epochs, number of epochs, and signal-to-noise ratio. Some features showed angular extensions of several mas, which degraded accuracy of proper motion measurements. However, the overwhelming majority of the spots were essentially point like and unresolved on the largest EVN or VLBA baselines. Several features were present only on a limited number of epochs due to the strong variability and limited lifetime of the maser spots. Only seven spots were detected at six epochs, the largest number of observing epochs, at 1665 MHz and three spots at 1667 MHz. These numbers are limited by the relatively low sensitivity of the 5-min snapshots of the VLBA observations in 1998 (Slysh et al. 2001, 2002). The proper motion was determined by the least-square linear fitting to the position data for each epoch. For 1665-MHz maser spots the mean proper motion of all the spots relative to the reference feature is 41 ± 25 μas per month or 4.3 ± 2.0 km s^{-1}. The mean proper motion of 1667-MHz maser spots is 102 ± 76 μas per month or 12 ± 8.6 km s^{-1}. The larger error for 1667-MHz measurements is due to the weakness of 1667-MHz features compared to 1665-MHz features. These values were obtained for the proper motion of the maser spots which were present on five or six epochs: 22 spots at 1665 MHz and 17 spots at 1667 MHz. A lower number of epochs generally resulted in larger errors. The scatter of data here is due to deviation of data points from fitted straight lines corresponding to constant-velocity motion. Our analysis has shown that the proper motion of most of the maser spots is within the error bars. Several spots show proper motion above 6σ: at 1665 MHz, these are spots with radial velocities 3.90, 9.36 and 7.35 km s^{-1}. Their proper motion is between 3.6 and 5 km s^{-1}; 1667 MHz features at 13.74, 8.07, 5.63 and 5.44 km s^{-1} have proper motions between 13 and 2.2 km s^{-1}.

Simultaneously with the huge 1000-Jy flare in 2003 (Alakoz et al. 2005), many numerous weaker spots have appeared around VLA2 in both 1665 and 1667 MHz transitions, Fig. 5. The proper motion data for these spots is based only on four epochs since the first two epochs took place before the onset of the flare. In spite of the large radial velocity dispersion, the tangential velocity of flare features derived from the four-epoch proper motion, is not much different from that of the whole sample.

3.2.3 *Errors of the proper motion*

As a check of the accuracy of proper motion measurements, one can look at the proper motion of individual σ components of Zeeman pairs. Since the components come from the same position (Slysh & Migenes 2006), they most likely share equal proper motion. At least for the case of ideal point source maser spots, since it is possible for the velocities of Zeeman components to be different beyond the level predicted from signal to noise arguments alone. At 1665 MHz, there are Zeeman pairs 9.37/12.45 and 5.25/7.29 km s^{-1}. The difference in the proper motion of the σ components is 3.8 ± 3.4 and 2.7 ± 2.9 km s^{-1}, respectively. The difference is within the error box, and that confirms the typical accuracy of the velocity of several km s^{-1}. Similarly, at 1667 MHz the maser spots at 5.44 and 8.07 km s^{-1} are at the same location and form a Zeeman pair with the magnetic field strength of 7.4 mG. Again, they most likely share the same proper motion of 2.2 km s^{-1}, with a difference in the tangential velocities less than 1.9 km s^{-1}. For Zeeman pairs from two-epoch measurements by Fish & Reid (2007), the difference of the proper motion can be inferred by inspecting the tables of maser spot positions in 2001 (Fish et al. 2005) and 2004 (Fish & Reid 2007). For Zeeman pairs common to both tables, the difference of the proper motion between σ components is close to zero, as it should be, but the scatter is 4.6 km s^{-1}. This value can be taken as the error of velocity in these two-epoch measurements, rather than 0.2 km s^{-1} estimated by Fish & Reid (2007). This median error estimate was identified as a random error given by the uncertainties in determining position centroids. Similar conclusion can be drawn from comparison of the proper motion of RHC and LHC components of linearly polarized maser spots. The difference of the proper motions is not zero as expected from physical arguments. It is of the order of several km s^{-1} for different spots, independent on the flux. The difference of the proper motion of circularly polarized components of linearly polarized maser spots of several km s^{-1} was also noticed in Fish & Reid (2007) and Fish et al. (2005) data. The difference between proper motion of independent circularly polarized components of maser spots, originating at the physically coinciding positions, is up to an order of magnitude larger than the errors calculated from noise contribution. The cause of this discrepancy probably lies in calibration errors and incomplete uv-coverage.

3.2.4 *Detections of the proper motion*

We have not detected proper motion of maser spots exceeding 2–10 km s^{-1}, except in the $N_1 - N_3$ complex. There are two special cases, and both concern the strongest 1665-MHz flare features N_1 and N_2. Fish & Reid (2007) based on their two-epoch proper motion measurements, erroneously identified N_1 in 2004 data with the bright precursor feature P_1 in 2001 data. They assumed that N_1 and P_1 are the same features, with slightly changed radial velocity and position, and deduced tangential velocity of about 50 km s^{-1} for N_1/P_1 pair. Our more extensive six-epoch data show that P_1 and N_1 are different features, P_1 present only in 2001, and N_1 present in the last four epochs, at a position distinctly different from the position of P_1. N_1 moves very slowly, with a tangential velocity (relative to A) 6.4 ± 1.8 km s^{-1} (3.5σ detection), that is much less than 50 km s^{-1}, claimed by Fish & Reid (2007). N_2 soon after onset of the flare became the strongest feature in the spectrum, and shows a rather large tangential motion, with the velocity 13.8 ± 2.2 km s^{-1} (more than 6σ detection) at the position angle $-33° \pm 9°$, roughly in the direction of the feature N_3. In Fig. 6, N_1 is at the position (0, 0), and N_2 is located just at the lower edge of the extended spot N_3.

This super-resolution map was made with 2 mas restoring beam, shown in the lower left corner. The motion of the compact bright spot N_2 along the slightly curved low brightness filament N_3 possibly reveals an excitation shock traced by the spot N_2.

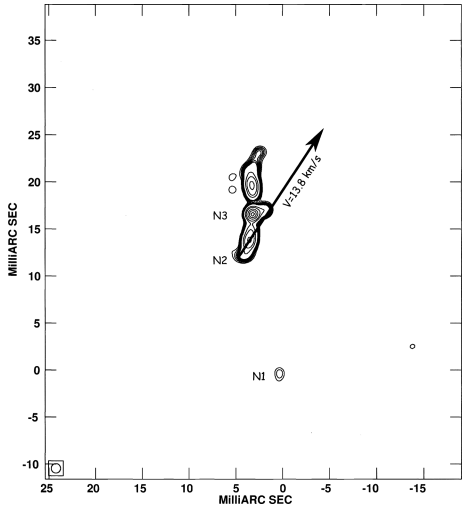

Figure 6. Super-resolution map of the maser spots N_1 to N_3 with the restoring beam 2 mas. Contours at 0.4, 0.5, 0.6, 0.7, 0.8, 0.9, 1, 2, 3, 5, 7 and 9 times the peak flux of 3.54 J_y/b. N_1 is at the position (0, 0) and N_2 is at the lower edge of the filamentary spot N_3. The arrow shows direction of the tangential motion of N_2.

3.2.5 Comparison with other proper motion measurements

Almost all previous proper motion studies of OH masers were based on two-epoch observations. As was stated earlier, it is impossible to detect from two-epoch VLBI data non-linear motion of the maser spots, such as accelerated or curved motion. Multi-epoch observations such as presented in this paper do allow to measure non-linear motion. In a linear fit, the scatter of data points would be due to the combined effects of non-linear motion and system noise. We have measured the mean linear motion of $4.3 \pm 2.0\,\mathrm{km\,s^{-1}}$ at 1665 MHz for all spots, relative to the reference spot *A*. The non-zero average velocity $4.3\,\mathrm{km\,s^{-1}}$ may result from the motion of the reference spot. However, the scatter $2.0\,\mathrm{km\,s^{-1}}$ is too large to make the result statistically significant. In the past measurements of the OH maser in W75N, a proper motion of $3.4 \pm 2.1\,\mathrm{km\,s^{-1}}$ was reported (Fish & Reid 2007), which is practically the same as our result. It should be noted that maser spot positions from these two epochs were included in our six-epoch Table 1, and used with our EVN results. The difference is that we found that the observed scatter is due to the noise, while Fish & Reid (2007) regard it as the real speed of maser spots. The reason is that our estimated error due to system noise is larger than estimated by these authors. They claim uncertainty of the proper motion $0.2\,\mathrm{km\,s^{-1}}$ (due to random errors in position) which is an order of magnitude less than our estimate. Because of the position errors, we were unable to measure reliably not only non-linear motion, but also the linear motion of most of the maser spots.

No other OH-maser proper motion study has covered a timespan of 8 yr or as many as six measurements. It may not seem quite clear how increasing the time base of observations may be of use because of the relatively short lifetime of individual spots. In order to identify and follow the spots in time, it is necessary to have measurements much closer spaced in time. Our data suggest that 6–8 month intervals is a reasonable time interval. For this study, the interval between the first three epochs carries the greatest identification uncertainty. In principle, it should be possible to discriminate between real motion, systematic errors due to calibration and poor *uv*-coverage with such a data base of high-resolution observations. But the proper motion of OH maser spots in W75N is less than several $\mathrm{km\,s^{-1}}$. For sources exhibiting higher proper motion a data base of this length of time and quality could reduce the scatter significantly providing more reliable estimate. We are presently examining other high-mass star-forming regions for which we have data and there are published results, to check if a similar study is possible.

3.3 Zeeman splitting as the origin of the large velocity range for VLA2

The HV features extend from 17 to $30\,\mathrm{km\,s^{-1}}$ and from –12.5 to $0\,\mathrm{km\,s^{-1}}$ at 1665 MHz; at 1667 MHz, two HV features at 15 and $21.5\,\mathrm{km\,s^{-1}}$ were present during the last three epochs (their radial velocity was outside the velocity coverage of the three epochs of VLBA observations), but not necessarily in all three EVN epochs. No motion of HV features was detected, and was found to be less than about $10\,\mathrm{km\,s^{-1}}$. HV features had both positive and negative radial velocities and are located only near VLA2, close to the bright flare features N_1 and N_2. The velocity range and mean radial velocity were 43 and $9\,\mathrm{km\,s^{-1}}$ at 1665 MHz, and 24 and $10\,\mathrm{km\,s^{-1}}$ at 1667 MHz, respectively (Fig. 4). The mean radial velocity is about the same as the radial velocity of other molecular tracers of the W75N region. The velocity range of OH masers is an order of magnitude greater than the molecular thermal line width, and should be compared with the low tangential velocity measured by the proper motion technique. The velocity difference between HV features does not seem to be related to their spatial separation. Near VLA2 very large radial velocity gradients are found. For example, 1665 MHz feature at $25.9\,\mathrm{km\,s^{-1}}$ is located only 6.45 mas (12.9 au) from N_1, while the radial velocity difference is large, about $24\,\mathrm{km\,s^{-1}}$, and corresponds to the radial velocity gradient of $1.8\,\mathrm{km\,s^{-1}\,au^{-1}}$. This is a very high value for the gradient compared to the velocity gradient in molecular clouds, where typical turbulent velocity gradients are of the order of 10^{-3}–$10^{-5}\,\mathrm{km\,s^{-1}\,au^{-1}}$. The radial velocity gradient of the OH maser spots associated with VLA1 is about $2 \times 10^{-3}\,\mathrm{km\,s^{-1}\,au^{-1}}$ or three orders of magnitude lower. For the kinematic origin of the high radial velocity range, it is difficult to reconcile its high value with the low transverse velocity. One may speculate that masers have a special geometry like cylinders, emitting and moving along their axis, and only maser cylinders moving in the direction on or away from observer are seen. Cometary tails may serve as examples of such cylinders. If the masers originate in comet-tail-like straight tails, the maser emission will be highly directed along the axis of cylinders because of larger optical depth, and are visible only from those tails which are directed towards the observer. This must be a small portion of the numerous comet-like objects orbiting parent stars and forming a cloud of comets similar to the Oort cloud in the Solar system. An alternative and more plausible explanation of the large radial velocity dispersion and low transverse velocity is that the velocity dispersion is not kinematic, but is caused by a large Zeeman splitting. This assumption looks reasonable, since a magnetic field strength of only 72 mG is required for the Zeeman splitting to equal the velocity difference $43\,\mathrm{km\,s^{-1}}$ at 1665 MHz, and 68 mG for the Zeeman splitting to equal the velocity difference $24\,\mathrm{km\,s^{-1}}$ at 1667 MHz. This is about twice the value 40 mG of the magnetic field strength measured during the previous, weaker flare in 2000–2001 (Slysh & Migenes 2006) confirmed by Fish & Reid (2007). The flare in 2003–2007 was an order of magnitude stronger than the precursor, so a magnetic field enhancement by another factor of 2 is possible. No Zeeman pairs with such a large radial velocity splitting were found in the new flare data. Most of the features are single, 100 per cent elliptically

polarized as would be expected for Zeeman splitting. However, no counterparts corresponding either to σ components or to π components were found in the data. The LHC-polarized feature at the large negative velocity can be a σ^{-1} component corresponding to an undetected σ^{+1} component of a Zeeman pair at a positive velocity. Only several Zeeman pairs with a weak magnetic field of about 5 mG, consisting of two circularly polarized σ components were found, the same as those reported for features not related to flare, near VLA1 (Slysh & Migenes 2006; Fish et al. 2005; Fish & Reid 2007). The strong inequality in intensity of Zeeman components is common in OH masers (Fish & Reid 2006). For pairs of weak features, the intensity of a weaker component may fall below the detection limit. Thus, the low proper motion and large velocity gradient are consistent with the Zeeman splitting of flare-related features in a strong magnetic field of about 70 mG.

4 DISCUSSION

One of the problems in maser studies is the nature of the maser spots. There are different opinions on this issue (Goddi et al. 2006). A simple model of an individual maser spots is that they are physical clumps of material, moving with velocities of several km s^{-1} (Bloemhof, Reid & Moran 1992) in an expanding shell or in a Keplerian disc. In one of the models, it was suggested that the maser spots originate in atmospheres of icy planets or of their moons orbiting central stars (Slysh et al. 1999). Another model for the maser spots assumes that they are simply the product of favourable lines of sight for coherent amplification within a larger turbulent molecular cloud Deguchi (1982). A combination of two models was proposed by Fish & Reid (2006) who suggested that it is 10^{15}-cm size physical clumps of matter housing clusters of maser spots, which are moving. The maser spots themselves, which are much smaller, indicate favourable coherent amplification lines of sight in the continuous turbulent clumps.

Present results are consistent with a model of OH maser consisting of stationary or slowly moving objects, whose maser emission is energized by a shock wave. This explains the observed 'Christmas tree' appearance of the intensity variations. The maser spots flash in a certain region of the whole maser, and shine for a period from months to years. As the shock is moving, new spots are energized and become masers. The speed of the shock may be estimated from the positive detection of proper motion of the brightest spot N_2 13.8 ± 2.2 km s^{-1} moving along the weak linear spot N_3. The spot N_3 is a filament about 9-mas long, with the velocity gradient of 0.09 km s^{-1} au^{-1}. Similar filaments are present in W75N such as spectral features *J* and *K* (Slysh et al. 2002), also with the velocity gradient. The speed of about 15 km s^{-1} may correspond to the motion of a MHD shock along the filament as suggested by Alakoz et al. (2005) from different arguments. It is not clear how the fading of some spots during the flare can be explained in such a model of shock excitation. The fading spots *J*, *K* and *L* are located very far from the assumed centre of activity VLA2 where all flaring spots are concentrated, at the projected distance 700–2200 au. This requires the exciting shock to have an unrealistic velocity 1000–4000 km s^{-1}. Therefore, the shocks cannot be the cause of the fading during the flare event, and some other agent may be responsible. Dissociation of maser molecules by a flash of ultraviolet radiation from the star could cause the maser fading provided that the extinction of the radiation is not too large. However, more likely the dimming of the features *J*, *K* and *L* is not related to the flare of 2003. The cause of dimming is probably internal, related to aging of the maser spots and their expansion. The older *Multi-Element Radio Linked Interferometer Network (MERLIN)* data of Hutawarakorn, Cohen & Brebner (2002) for 1986 and 1993 show *J* and *K* to be an order of magnitude stronger than in the period from 1998 to 2006. The 1667 MHz spot *L* was at maximum between 1993 and 1998, also well before the onset of the huge flare of 2003. These maser spots show a continuous slow decline not related to the flare near VLA2, with a time-scale of about 10 yr.

The estimated enhancement of the magnetic field strength up to 70 mG (Section 3.3) during the maser emission flare was deduced from the large velocity range of spectral features, mainly from HV features. This estimate can be tested by similar observations of masers in W75N on paramagnetic molecules, such as methanol, provided they co-exist with OH masers. In W75N, the velocity range of the 6.7 GHz methanol masers is only 5.8 km s^{-1} (Minier et al. 2000), which is much less than the velocity range of OH masers. Methanol as a non-paramagnetic molecule is not affected by the Zeeman splitting, so the observed velocity range can be attributed to the kinematic motion. If it were possible to exclude the effect of Zeeman splitting from OH data (demagnetize) the velocity range would become comparable to the methanol velocity range (Szymczak & Gérard 2004). All methanol maser spots are aligned with the OH maser structure near the ultracompact H II region VLA1 (Minier et al. 2000). Results of VLBI observations (Minier et al. 2000) show that the velocity range is due to the organized large-scale motion, similar to OH masers near VLA1. The magnetic field is weaker there, and Zeeman splitting does not increase much the velocity dispersion. No methanol maser spots have been found near VLA2 where most of the activity was observed, so there is no data on kinematic velocity dispersion near VLA2. On the other hand, there are numerous variable masers of another paramagnetic molecule H_2O, both near VLA1 and VLA2. The velocity range of the masers associated with VLA1 is 6.6 km s^{-1}, while the velocity range of the masers associated with VLA2 is 19.1 km s^{-1} (Torrelles et al. 1997). A similar velocity range was found by Lekht et al. (2007): 5 km s^{-1} for masers located near VLA1 and about 15 km s^{-1} for masers associated with VLA2. The velocity range of H_2O masers associated with VLA1 is the same as that of methanol masers. This must be compared with the velocity ranges of OH masers: 8.5 km s^{-1} for VLA1 and 43 km s^{-1} for VLA2. Both are larger than the velocity ranges of H_2O masers, although for VLA2 the OH-masers difference is more pronounced. The spectrum of H_2O is not affected by splitting in the magnetic field of reasonable strength. Therefore, the H_2O velocity ranges must be of kinematic origin, and if both species co-exist, the larger velocity range of OH masers partly is due to the kinematic motion and partly due to the Zeeman splitting.

5 CONCLUSIONS

(i) During the OH maser flare of 2003 two new, strong 1665 MHz spectral features arose, as well as numerous weaker 1665 and 1667 MHz features, including some high-velocity features. The intensity of the flare features varied in a large range with the time-scale of months, while their radial velocity remained stable.

(ii) The position of OH maser spots is quasi-stationary, with the transverse velocity an order of magnitude less than the radial velocity range. The two strongest maser spots have the largest tangential velocity, of about 10 km s^{-1}.

(iii) The observed large radial velocity range of the OH maser spots near ultracompact H II region VLA2 is due to the Zeeman splitting in the strong magnetic field of about 70 mG produced by the central star during the flare of OH maser emission.

(iv) The maser spots trace position of MHD-shocks travelling in weak emitting filaments. The shocks are generated in the immediate vicinity of young massive stars that excite ultracompact H II regions.

ACKNOWLEDGMENTS

We acknowledge JIVE staff for the efficient treatment of EVN data. The European VLBI network is a joint facility of European, Chinese, South African and other radio astronomy institutes funded by their national research councils. Kalyazin 64-m radio telescope is a joint facility of OKB MEI and Astro Space Centre. The work of AVA and VIS was partly supported by RFBR Grant No. 07-02-00248.

REFERENCES

Alakoz A. V., Slysh V. I., Popov M. V., Val'tts I. E., 2005, Astron. Lett., 31, 375
Bloemhof E. E., Reid M. J., Moran J. M., 1992, ApJ, 397, 500
Deguchi S., 1982, ApJ, 259, 634
Fish V. L., Reid M. J., 2006, ApJS, 164, 99
Fish V. L., Reid M. J., 2007, ApJ, 656, 943
Fish V. L., Reid M. J., Argon A. L., Zheng X.-W., 2005, ApJS, 160, 220
Goddi C., Moscadelli L., Torrelles J. M., Uscanga L., Cesaroni R., 2006, A&A, 447, L9
Goedhart S., Gaylard M. J., van der Walt D. J., 2004, MNRAS, 355, 553
Hutawarakorn B., Cohen R. J., Brebner G. C., 2002, MNRAS, 330, 349
Lekht E. E., Slysh V. I., Krasnov V. V., 2007, Astron. Rep., 51, 967
Minier V., Booth R. S., Conway J. E., 2000, A&A, 362, 1093
Shepherd D. S., Kurtz S. E., Testi L., 2004, ApJ, 601, 952
Slysh V. I., Migenes V., 2006, MNRAS, 369, 1497
Slysh V. I., Val'tts I. E., Kalenskii S. V., Larionov G. M., 1999, Astron. Rep., 43, 657
Slysh V. I., Val'tts I. E., Migenes V., 2001, Astron. Rep., 45, 942
Slysh V. I., Migenes V., Val'tts I. E., Lyubchenko S. Yu., Horiuchi S., Altunin V. I., Fomalont E. B., Inoue M., 2002, ApJ, 564, 317
Szymczak M., Gérard E., 2004, A&A, 414, 235
Torrelles J. M., Gómez J. F., Rodríguez L. F., Ho Paul T. P., Curiel S., Vazquez R., 1997, ApJ, 489, 744
Yngvesson K. S., Cardiasmenos A. G., Shanley J. F., Ellder J., Rydbeck O. E. H., 1975, ApJ, 195, 91
Zhang H.-B E. J., Zhou J.-J., Zheng X.-W., Zhang X.-Z., Yang W.-J., 2005, Chinese J. Astron. Astrophys., 5, 557

This paper has been typeset from a TEX/LATEX file prepared by the author.